KTH Industrial Engineering and Management

NUMERICAL MODELLING OF A NOVEL PVT COLLECTOR AT CELL RESOLUTION

Gustav Schön

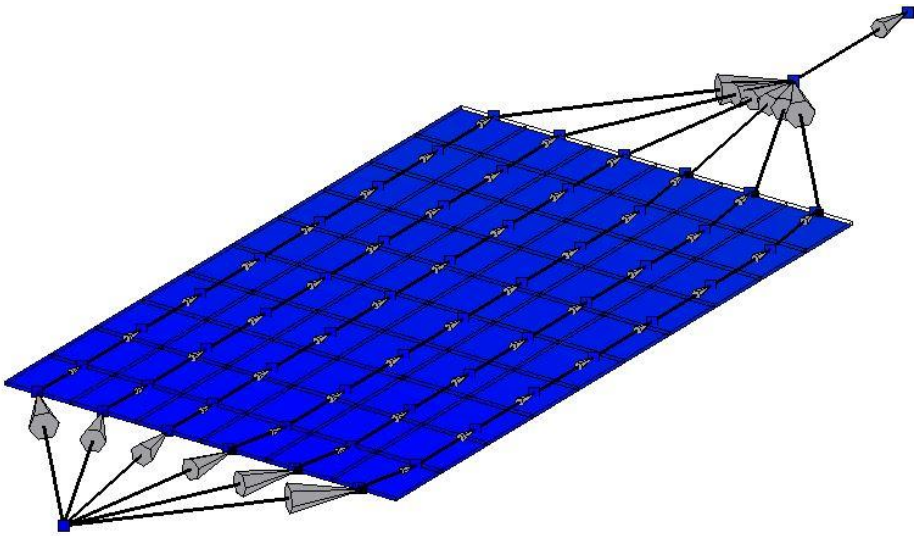

Master of Science Thesis

KTH School of Industrial Engineering and Management
Energy Technology EGI 2017-0033-MSC
Division of Applied Thermodynamics and Refrigeration
SE-100 44 STOCKHOLM

Master of Science Thesis EGI 2017-0033-MSC

KTH Industrial Engineering and Management

NUMERICAL MODELLING OF A NOVEL PVT COLLECTOR AT CELL RESOLUTION

Gustav Schön

Approved	Examiner	Supervisor
2016-06-01	Hatef Madani Larijani	Nelson Sommerfeldt
	Commissioner	Contact person
	Solhybrid i Småland	Magnus Johansson

Abstract

Solar photovoltaic-thermal (PVT) modules produce heat and power via a heat exchanger attached to the rear of the PV cells. The novel PVT collector in this study is previously untested and therefore its behaviour and thermo-electric performance due to fluid channel configuration and in various climate and operating conditions are unknown. Moreover, the working fluid flowing through the heat exchanger cause a temperature gradient across the module such that a cell near the inlet and a cell near the outlet may have significant temperature differences. PV cells are sensitive to temperature; however the most common way to simulate power output from a PVT is to use the average temperature and ignore the gradient. In this study, a single diode PV model is incorporated into a commercial thermal solver to co-simulate the thermal and electrical output of a novel PVT module design with cell level resolution.

The PVT system is modelled in steady state under various wind speeds, inlet temperatures, ambient temperatures, flow rates, irradiation, convection coefficients from coolant and back of the module and two different fluid channel configurations. The results show that of the controllable variables, the inlet temperature has the highest influence of the total power output and that a parallel flow of the fluid channel configuration is preferable. The difference between the cell resolution and the module resolution simulations do not motivate the use of a higher resolution numerical simulation.

Keywords

Photovoltaic, Thermal, Solar, Hybrid system, Ground Source Heat Pump, Energy, Renewable, Collector, Absorber, TAITherm, PVT, PV/Thermal

Sammanfattning

En kombinerad solcellspanel och solvärmefångare (PVT) producerar värme och elenergi på samma yta genom att en värmeväxlare upptar värmen från baksidan av solcellspanelen. Den PVT som berörs i denna studien är nyutvecklad och har aldrig tidigare testats, vilket medför att data för hur den beter sig samt dess termo-elektiska prestanda saknas för olika driftförhållanden samt flödeskonfigurationer. Vidare ger mediet som flödar genom värmeväxlaren upphov till en temperaturgradient, vilken kan innebära en påtaglig skillnad i temperatur mellan solcellerna i solcellspanelen vid mediets in- respektive utlopp. Trots solcellers temperaturkänslighet, så sker simulering i allmänhet med avseende på panelens medeltemperatur istället för att hänsyn tas till denna temperaturgradient. I den här studien implementeras en så kallad ”single diode”-modell i en kommersiell numerisk mjukvara termiska beräkningar för att samsimulera termiskt och elektriskt effektuttag ur den nyutvecklade PVT-designen. Designen modelleras statiskt under givna variationer av vindhastighet, inloppstemperatur, omgivande temperatur, flödeshastighet, solinstrålning och konvektionskoefficienter för mediet samt baksidan av modulen. Resultaten visar att kontrollerbara variabler som inloppstemperatur har högst inverkan på den totala effekten samt att en parallell flödeskonfiguration lämpar sig bäst. Studien visar också att skillnaden mellan simulering på cellnivå och modulnivå inte motiverar en numerisk beräkningsmetod med upplösning satt till solcellsnivå.

Acknowledgements

I want to thank my supervisor Nelson Sommerfeldt for his excellent support throughout this project. His feedback, superior language skills and patience cannot be valued enough. I also want to thank all my friends and family who has encouraged me when the lack of motivation has overwhelmed me.

This work was financed by Mistra Innovation, project number MI15.18.

Contents

List of Figures

List of Tables

Nomenclature

A_{cells}	Total area of PV cells in module
A_{module}	Area of module
Ab_{eff}	Effective absorption factor
Ab_{cell}	Absorption factor of a PV cell
a	Modified ideality factor
C_{ratio}	Coverage ratio
C_p	Specific heat
C_c	Specific heat of the collector plate
E_g	Material band gap
$E_{g,ref}$	Material band gap reference
$\dot{E}_{pv}$	Photovoltaic output power per unit cell area
F_I	Dependency of electrical efficiency on irradiation
F_T	Dependency of electrical efficiency on cell temperature
G	Irradiation
h_{wind}	Convective heat transfer coefficient at the collector outside
$h_{r,c\text{-}a}$	Radiation heat transfer coefficient, collector to ambient
$h_{c\text{-}f}$	Radiation heat transfer coefficient, collector to fluid
I	Current
I_L	Light current
I_D	Diode reverse saturation current
k	Boltzmann's constant
M	Air mass modifier
M_{ref}	Air mass modifier reference
$\dot{m}$	Mass flow
N_S	Number of cells
n_I	Ideality factor
q	Electron charge
R_s	Series resistance
R_{sh}	Shunt resistance
S	Absorbed irradiance
S_{ref}	Absorbed irradiance reference
T_{cell}	Temperature of cell
T_{in}	Inlet temperature
T_{out}	Outlet temperature
T_a	Air temperature
T_c	Collector temperature
T_f	Water flow temperature
V	Voltage
α_c	Absorptivity of the collector
β	Temperature coefficient of electrical efficiency
δ_c	Thickness of the collector plate
η_e	Electrical efficiency
η_e^{STC}	Electrical efficiency at standard conditions
η_{power}	Average efficiency of conventional power plants
η_q	Quantified efficiency
η_t	Thermal efficiency
ρ_c	Density of the collector plate

1 Introduction

Modern society is facing possibly the greatest challenge in history; to reduce effect of global warming to 1.5°C (European Commission, 2016). This challenge entails the need to bring forth all technologies capable of contributing to such. Solar energy is well known to have a great potential as there is no cost of fuel and it is available for everyone. Today, most commercial solar energy collectors are either photovoltaic (PV) or thermal and when used together are usually placed side to side, resulting in low power to area efficiency. These are typically used in small houses or dwellings for heating purposes or powering home equipment. By combining the two techniques into one module, the photovoltaic thermal (PVT) module, the space efficiency can be increased and the manufacturing cost can be reduced (Chow, 2009). Another technical benefit of combining the two techniques is the possibility to reduce the cell temperature of the PV module since the electrical efficiency has a dependency on the cell temperature (Calise, et al., 2012) (Dalvand, et al., 2012).

The heat actively removed can then be used in a ground source heat pump (GSHP) system to charge a borehole in order to maintain the long-term average temperature in the ground (Bakker, et al., 2003). In this way, the temperature of the PVT module can be kept at a lower temperature than in a similar domestic water heating application and the borehole can be used as a seasonal storage (Bakker, et al., 2003). According to previous studies, a PVT module can reach an overall efficiency of between 45-87 percent (Chow, 2009) (Haurant, et al., 2014) whereas a common PV-module on the market has about 15 percent efficiency (Energimyndigheten, 2016) and above 20 percent for state of the art photovoltaic (Willeke & Weber, 2015).

1.1 Problem and objective

A unique PVT design is under development by Solhybrid i Småland AB which is built up by a glass-glass PV module joint with an aluminium back-panel allowing the fluid cooled by a GSHP to pass directly to the glass. Being a novel design, there is a lack of knowledge about how the module will perform, particularly under the conditions it would be exposed to in a GSHP system.

To better understand this PVT design, this paper seeks to answer the following questions:

- What are is the efficiency of the collector under various climate and operating conditions?
- What is the sensitivity of the collector to various operating conditions?
- Is there an influence from fluid channel configuration on thermal output?

Answering these questions about design brings up questions about the PVT modelling process. For example; does this difference impose the need for a cell resolution numerical method in systems modelling? How critical are convection models, particularly on the rear where there is a significant uncertainty about air flow? In the process of answering the primary questions above, these modelling issues will also be investigated.

1.2 Methodology and scope

To answer the questions outline above, the following process will be followed;

- A review of PVT design principles and previous research
- Construction of a numerical thermal model using commercial software
- Integration of an PV electrical model into the thermal model
- Sensitivity analysis

There are numerous potential PVT configurations, however this study is focused on the evaluation of a single flat plate, liquid cooled, PVT collector design from Solhybrid i Småland AB (hereafter referred to as Solhybrid). Flat plate is the most cost effective and common type of PVT collector for buildings, therefore the work is relevant for a wide audience (Zondag, 2008). The study will be done using computer simulations and given the early design phase is limited to steady state conditions. Validation with empirical measurements is left for future works.

2 Background

The modern solar PV module still has a rather low power output per unit area and therefore demands large surfaces for producing the power needed by a consumer. By joining the PV with a thermal collector into one PVT module the overall efficiency per unit area can be increased. The thermal collector is attached to the back of the PV so that heat absorbed from irradiance in the PV can be extracted and used in a domestic heating system. Meanwhile, the PV produces electrical power that can be used for various appliances. The combination may also have a lower life-cycle cost than having PV and thermal collectors side by side (Chow, 2003). PVT collectors have been investigated widely, and this chapter reviews that research and describes the critical design principles

Most designs of PVT modules operate on the same basic principles, where the PV layer acts as an absorber of solar radiation, a working fluid is passed on the rear, and can then be wrapped in insulation and/or glazing. Most commercial designs are similar with an absorber fixed to the back of the PV cells, but with different design of the heat absorber and if they are glazed or not. The most common types of absorber designs are; the roll bond, parallel duct, and the sheet-and-tube (Charalambous, et al., 2007) (del Pero, et al., 2014) (Chow, 2009). Cross-sectional views of the sheet-and-tube and parallel duct designs are shown in Figure 1. The roll bond type is not shown since it is more of a manufacturing technique and has a variety of complex designs. Sheet-and-tube collector types are the most common according to Calise et al. (2012).

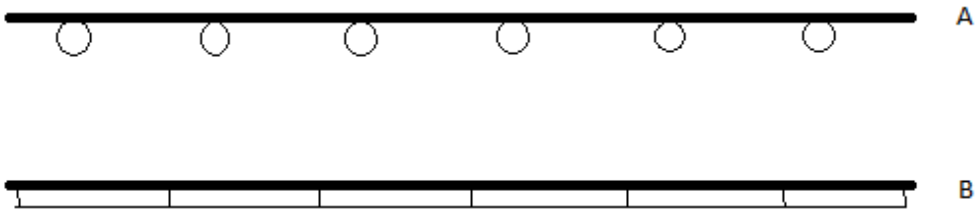

Figure 1 Two of three common PVT designs A: Sheet-and-tube and B: Parallel duct

Zondag (2008) notes that the most basic technique for manufacturing PVT collectors is to either glue PV cells or a commercial PV-module together with a commercial thermal collector, although both ways have their drawbacks. The first option comes with the potential consequence of insufficient electrical insulation and protection from the ambient. The second option comes with the consequence of high thermal resistance, a gluing step which is not optimal for commercial manufacturing and high reflection losses with the white module backing.

Sandnes & Rekstad (2002) compared three collector configurations, of which, one is a glazed type, in terms of thermal performance when combining a solar thermal collector with PVs into a PVT module. The two unglazed configurations were compared to the pure thermal absorber with the combined PVT module. A conclusion was made that the available energy for the thermal absorber was reduced by the fraction of energy converted to electricity in the PV-cells. Also, the optical absorption was lower with the PV-cells than with the black absorber plate.

2.1 Photovoltaic solar collectors

The photovoltaic cell transforms photon energy corresponding to a specific energy band gap to electric energy by exciting electrons in the cell. The photon energy outside of this gap, about 85-90 percent, are not transformed into electric energy and are either reflected or turned into heat in the PV-module (Chow, 2009) (Ji, et al., 2007). About 80 percent of the energy received by the PV-module is converted to heat, which causes the cell temperature to rise and can result in high operating temperatures if not cooled (Gómez, 2009)

(Chow, 2009). The efficiency drops about 0.45 percent per kelvin (K) for silicon cells meaning that a cell that has 15 percent efficiency at 25°C will have only 11.6 percent efficiency at 75°C (Calise, et al., 2012) (Chow, 2009). There also exists a risk of permanent structural damage to the module when thermal stress remains for long periods (Chow, 2009).

2.1.1 Physical design of PV-modules

The arrangement of encapsulates varies depending on the manufacturer, but the typical PV-module is arranged as glass-EVA-cell-EVA-Tedlar, where EVA is an abbreviation of ethyl vinyl acetate and Tedlar is the trade name for a plastic film product by DuPont. In the PVT under development by Solhybrid and used in this study, the Tedlar is replaced by glass in the following layers: glass-EVA-cell-EVA-glass. The glass used is a low iron content type in order to reduce the transmitting losses and the EVA is assumed to have similar optical properties as the glass (Santbergen & van Zolingen, 2008).

2.1.2 Electrical efficiency of PV

There are several different types of PV modelling techniques with different efficiencies and thermal behaviour. In this thesis, c-Si cells are considered since they are the most common type and also the type intended to be used in the module identified in the scope.

According to (Santbergen & van Zolingen, 2008) the electrical efficiency η_e can be estimated with (1);

$$\eta_e = \eta_e^{STC} F_I F_T \quad (1)$$

where F_I (shown in Figure 2) describes the dependency of the electrical efficiency on irradiance I_{sun} and F_T the dependency on cell temperature T_{cell} and η_e^{STC} the collector efficiency at STC. In the practical temperature range; F_T can be considered linear and dependent on the temperature coefficient of the electrical efficiency β according to;

$$F_T = 1 + \beta(T_{cell} - 25°C) \quad (2)$$

where β for c-Si cells is normally close to -0.0045/°C and for single-junction CIGS cells is -0.002/°C (Santbergen, et al., 2010) (Santbergen & van Zolingen, 2008) (Green, 1982).

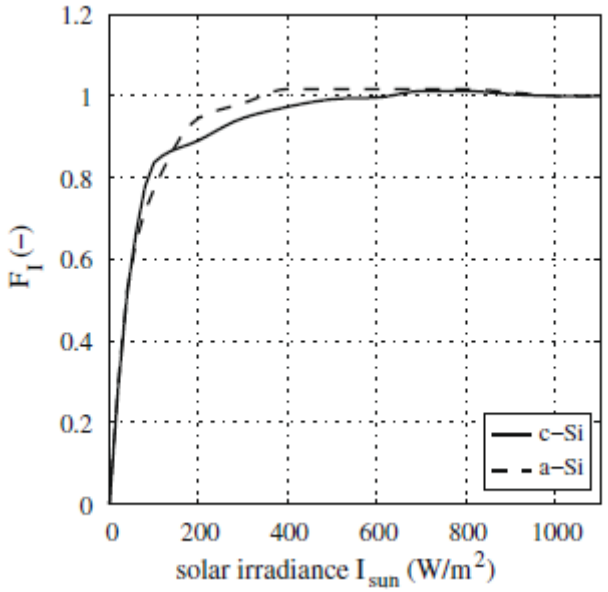

Figure 2 The solar irradiance factor F_I as function of I_{sun} (Santbergen, et al, 2010)

Combining equation (1) and (2) gives the following expression;

$$\eta_e = \eta_e^{STC} F_I (1 + \beta (T_{cell} - 25°C) \quad (3)$$

which can be used to determine the efficiency dependent on the cell temperature. The efficiency can also be calculated by determining the ratio between power output per square meter of the PV module and the incident irradiation. The final efficiency of PV modules is affected by the cell-to-module ratio C_{ratio} according to equation (4) also referred to as coverage factor or packing factor. The cell-to-module ratio is often in the range between 92-96 percent. (Santbergen, et al., 2010).

$$C_{ratio} = \frac{A_{cells}}{A_{module}} \quad (4)$$

Calculating the electrical efficiency can be done using;

$$\eta_{el} = \frac{VI}{GA_{module}} \quad (5)$$

where V and I are the voltage and current for the PV cell or PV module, G the irradiance and A_{module} the area of the module.

2.1.3 Single diode Model

The single diode model can be used to determine the power output for a module or individual cells. An electrical diagram of the single diode model is shown in Figure 3 where I_L, I_D, I_{sh}, R_{sh} and R_s refer to light current, diode reverse saturation current, shunt current, shunt resistance and series resistance respectively. The light current represents the current generated when the sun hits the PV cell.

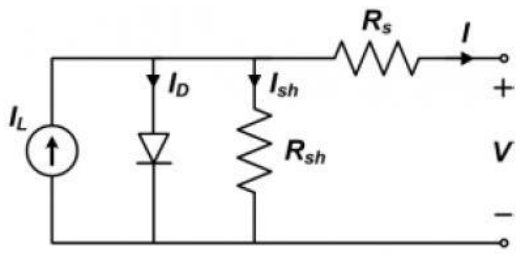

Figure 3 Single Diode Model

The corresponding equation (6), described in the paper of (De Soto, 2004), forms the shape of the IV-curve. The IV-curve will then be used to determine the voltage or current at given conditions where *a* is the ideality factor.

$$I = I_L - I_D \left[exp\left(\frac{V + IR_s}{a}\right) - 1 \right] - \frac{V + IR_s}{R_{sh}} \quad (6)$$

The light current, diode reverse saturation current and modified ideality factor are all temperature dependent and given by equations (7), (8) and (9).

$$\mathrm{a} = \frac{N_S n_I k T_{cell}}{q} \quad (7)$$

$$\frac{I_D}{I_{D,ref}} = \left(\frac{T_{cell}}{T_{cell,ref}}\right)^3 \exp\left(\frac{1}{k}\left(\frac{E_{g,ref}}{T_{cell,ref}} - \frac{E_g}{T_{cell}}\right)\right) \quad (8)$$

$$I_L = \frac{S}{S_{ref}}\frac{M}{M_{ref}}\left(I_{L,ref} + \alpha_{I_{sc}}\left(T_{pvcell} - T_{cell,ref}\right)\right) \quad (9)$$

The light current is dependent on the material band gap E_g and given by equation (10) which also is temperature dependent. The reference band gap $E_{g,ref}$ is given for silicon cells to be 1.121 eV. k and q are the Boltzmann´s constant and electron charge respectively.

$$\frac{E_g}{E_{g,ref}} = 1 - 0.0002677\left(T_{cell} - T_{cell,ref}\right) \quad (10)$$

Moreover, the light current has a strict dependency on the ratio of absorbed radiation (S/S_{ref}) given by equation (11). The air mass modifier (M/M_{ref}) is in this report assumed to be one as the study of irradiance is parametric. G and G_{ref} are the current and reference irradiations.

$$\frac{S}{S_{ref}} = \frac{G}{G_{ref}} \quad (11)$$

$I_{D,ref}$, $I_{L,ref}$, R_s, and R_{sh} are reference parameters determined through a set of nonlinear equations using data provided by the manufacturer while the n_I is set to be 1.2.

2.2 Glazed vs. Unglazed PVT

Glazed and unglazed PVTs each have their benefits and drawbacks. Glazed PVT have a higher thermal output as the glazing adds a layer of air that will act as insulation in front of the PVT. However, the glass adds an additional layer of resistance for the irradiation and decreases the incident irradiation on the PV-cells by approximately 5%. (Santbergen, et al., 2010) (Sandnes & Rekstad, 2002)

Which type of design chosen depends on the thermal and electrical user demand and often on the climatic condition (Chow, et al., 2009). Since unglazed PVT provides more electrical energy as compared to glazed PVT it will also be expected to have a higher exergy output (Fujisawa & Tatsuo, 1997).

2.3 Efficiency of PVT

The efficiency of a PVT is sometimes hard to compare since various papers use different approaches, but the annual thermal efficiency for PVT liquid systems is in the range between 45-70 percent (Chow, 2009). According to Santbergen (2010), a low temperature of the inlet fluid is beneficial for the efficiency of the PVT-module, however if the temperature is lower in the PVT-collector than the ambient temperature condensation can occur. From a thermal collection aspect this is positive, but considerations must be made that condensation can result in damage to the module, especially when close to freezing temperatures (Holman, 2009). The uncovered and single covered sheet-and-tube collectors had a thermal efficiency of 52 and 58 percent respectively in a simulation study conducted by (Zondag, et al., 2002) and (Zondag, et al., 2003).

The thermal efficiency can be calculated through equation (12),

$$\eta_t = \frac{\dot{m} C_p (T_{out} - T_{in})}{G A_{module}} \quad (12)$$

where G is the incident solar irradiation, A the collector area, $\dot{m}$ the mass flow through absorber, C_p the specific heat capacity of the coolant. And the electrical efficiency through equation (4) in section 2.1.2

To compare the efficiency of different PVT designs one can sum the efficiencies of the PV-module and the absorber, but since electricity is considered more valuable due to the higher exergy, the efficiency can instead be estimated with the primary energy needed to produce electricity by using equation (13),

$$\eta_q = \frac{\eta_e}{\eta_{power}} + \eta_t \quad (13)$$

where η_{power} represents the electrical power generation efficiency of a conventional power plant. The average in Europe is 0.38 (Chow, 2009) (Tiwari, et al., 2006) (Huang, et al., 2001).

2.4 Absorption factor

The absorption factor is the total amount of solar radiation absorbed by the PVT where an effective absorption factor can be introduced to distinguish the difference between the total radiation absorbed and the amount available for thermal extraction. This distinction is also applicable to show the difference between a thermal collector and the PVT (Santbergen, et al., 2010).

Santbergen (2010) claims that the thermal absorption factor ($Ab_{thermal}$) is reduced to an effective absorption factor (Ab_{eff}) with the same amount as the electrical efficiency of the PV-module $Ab_{eff} = Ab_{thermal} - \eta_e$. By combining this equation with (3) for calculating the temperature dependent electrical efficiency, an effective absorption factor can be found for the working temperature of the PVT module.

Combining those gives equation **(14)**:

$$Ab_{eff}(T_{cell}) = Ab_{cell} - \eta_{el}^{STC}\{1 + \beta(T_{cell} - 25°C)\} \quad (14)$$

In the computational model developed by Santbergen and van Zolingen (2008) the roughness and multiple reflections of trapped irradiance, etc. of the PV-surface is considered and investigated to determine the absorption factor. The model described is a 2D numerical model where all layers between ambient to metal back contact of the PV-module are being considered, see Figure 4. (Santbergen & van Zolingen, 2008)

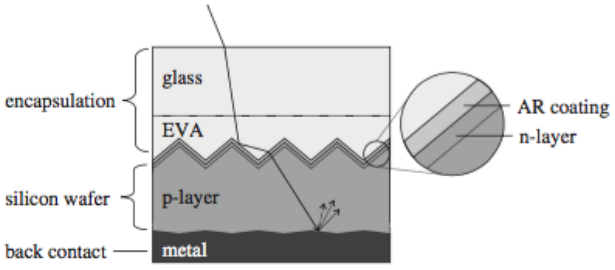

Figure 4 Layers in a PV-module (Santbergen & van Zolingen, 2008)

The absorption factor (Ab) for various types of PV cells ranges in-between 70-90 percent and the effective absorption factor (Ab_{eff}) between 60-80 percent after considerations have been taken for the energy transformed into electrical energy (Santbergen, et al., 2007) (Santbergen & van Zolingen, 2008)

Table 1 Typical values of absorption factor (Ab), effective absorption factor (Ab_{eff}) and emissivity ε of a spectrally selective absorber and of a PV laminate (Santbergen, 2008)

	Spectrally selective absorber	PV laminate
Ab (%)	95	70-90
Ab_{eff} (%)	95	60-80
ε (%)	12	85

Using the cell absorption factor (Ab_{cell}) presented in Table 2 the efficient absorption factor can be calculated by subtracting the electrical efficiency of the PV-module.

Table 2 Cell and effective absorption factor (Santbergen & van Zolingen, 2008)

	H-pattern planar	H-pattern textured	PUM textured	EWT textured
A_{cell} (%)	81.4	85.1	87.4	90.5
A_{eff} (%)	67.0	70.1	71.8	74.4

2.5 Heat exchangers in PVTs

As mentioned in section 2.1 the most common design is the sheet-and-tube, where the tubes are bonded or formed into to an absorber plate. In Figure 5 the tubes are arranged in such way that they have an equal spacing and create a parallel flow across the plate between the two headers. It is also common for there to be a single tube that snakes across the module, also known as a serpentine or series configuration. Because of the parallel design being symmetrical, the modelling of it can be simplified by just considering the heat flow along one of the tubes and assuming that there is no heat flow between the adjacent tubes (Calise, et al., 2012) (Chow, 2003) (Santbergen, et al., 2010). An assumption made by Chow while simulating claims that the losses of the absorbed solar energy will only occur through the front and back of the panel whilst the heat loss from the edges can be neglected for compact and thin panel designs. The design in Figure 5 will have a positive temperature gradient along the fluid flow due to accumulating heat transfer. (Chow, 2003).

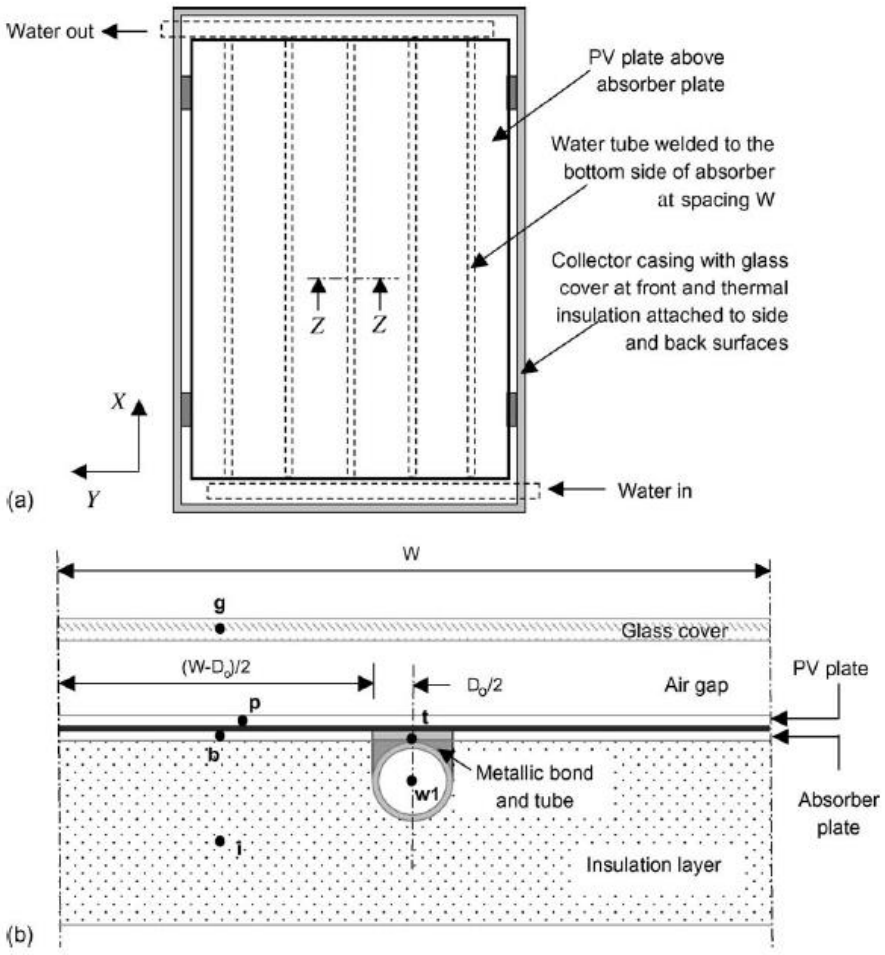

Figure 5 Sheet-and-tube PVT (Chow, 2003)

Ito, et al (2005), conducted an experiment with PV/thermal collectors using refrigerant as fluid in the heat exchanger. The experiment considered a roll-bond type PVT with refrigerant (R22) as coolant where two absorbers were considered; type one represents an aluminium roll-bond collector, type two had the same pattern but was modified by separating the inlet according to Figure 6. For type one the pressure drop between inlet and outlet was 350 kPa and for type two the pressure drop was 90 kPa for the same condenser temperature. The pressure drop will affect the power used by the pump and can therefore decrease the overall efficiency of a system of PVT and GSHP in conjunction.

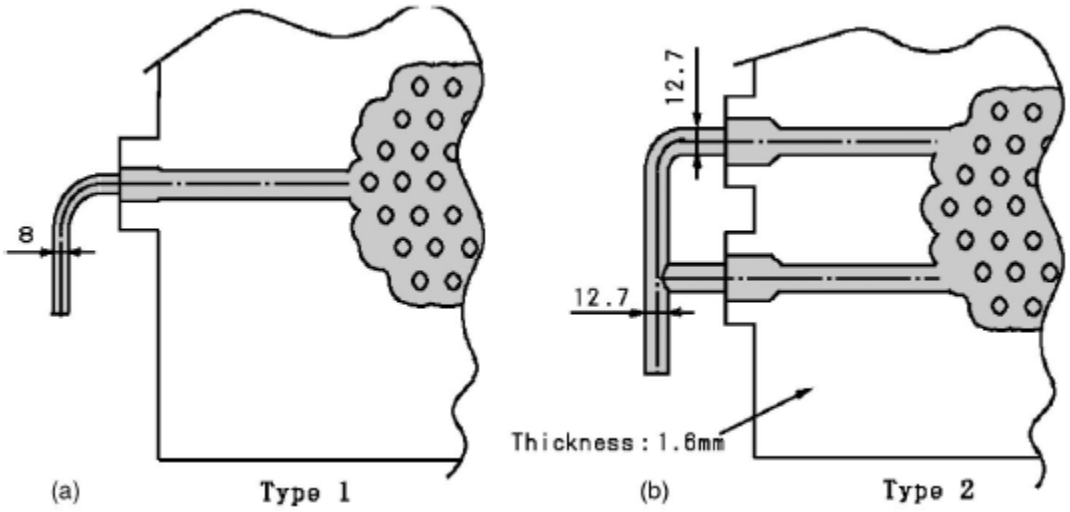

Figure 6 Roll-Bond pannels used as evaporators (Ito, et al., 2005)

A modified polyphenylenoxid (PPO) plastic absorber was used in the PVT by Sandnes & Rekstad (2002), shown in Figure 7. The absorber was a parallel duct design with ceramic granulate filled channels. The flow through the absorber was from top to bottom caused by gravity and as the water passes the ceramic, the flow is disturbed, causing mixing which enables a better heat transfer. The back of the absorber was insulated with 5 cm mineral wool. The PV-cells were not running while the thermal performance was examined (Sandnes & Rekstad, 2002). When tested, the average cell temperature was reduced from 52°C to 18°C when using cold water (10-12°C) in the absorber. During the experiment the average insolation was 749 W/m² and the ambient air temperature was 8-9°C (Sandnes & Rekstad, 2002).

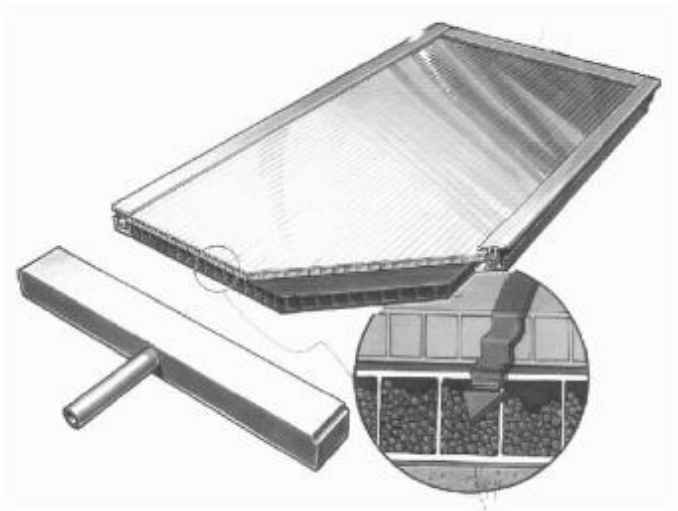

Figure 7 PPO plastic absorber (Sandnes & Rekstad, 2002)

Chow et al (2008) uses a modular flat-box aluminum type PVT according to Figure 8 where the liquid flows parallel in several aluminum channels. They claim this design improves heat transfer, flexibility and durability. The flexibility is due to the extruded water-channel modules that can be put together to fit any size of PV-module. The 24-hour thermal efficiency for this design reached around 28 percent. (Chow, et al.,

2008). By adding isolation on the back of the PVT, prevention can be made against heat losses to the environment. This can result in a higher manufacturing cost but higher thermal power output.

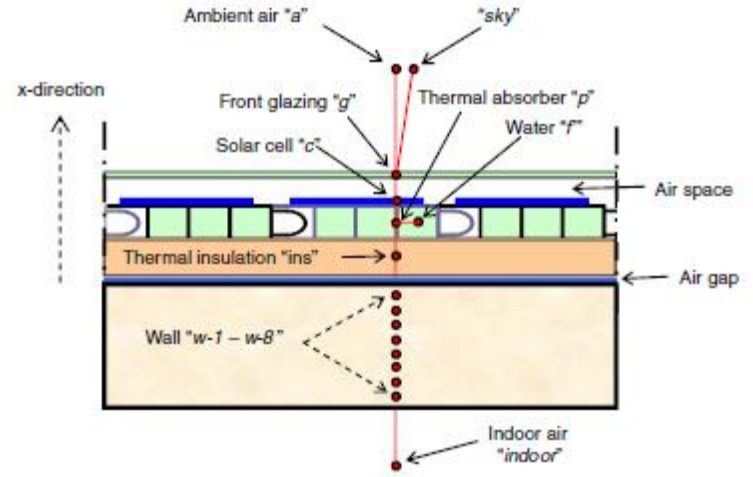

Figure 8 Modular flat-box type PVT (Chow, et al., 2008)

2.6 Computational/Numerical models

The diagrams in Figures 5 to 8 can be used to clarify the modelling approaches of PVT. For example, the PVT collector presented in Figure 5 is represented by seven nodes where the node "g" is represented by the glass cover, "p" the PV plate, "b" the thin plate absorber, "t" the metallic bonding between the plate absorber and the tube, "i" the insulating layer, "w1" the liquid in the tube and one node for the water leaving. (Chow, 2003).

Without the glass cover, Chow et al (2009) presented the following numerical equation (**15**):

$$\rho_c \delta_c C_c \frac{dT_c}{dt} = G\alpha_c - \dot{E}_{pv} + \left(h_{wind} + h_{r,c-a}\right)(T_a - T_c) + h_{c-f} A_f \left(T_f - T_c\right) + \frac{T_a - T_c}{R_{in}} \quad (15)$$

where ρ_c, δ_c and C_c are density, thickness and specific heat respectively of the collector plate. T_a, T_c and T_f are the temperature of ambient air, collector plate and water flow respectively, α_c is the absorptivity of the collector, $\dot{E}_{pv}$ is the photovoltaic output power per unit cell area, h_{wind}, $h_{r,c-a}$ and h_{c-f} are the convective heat transfer coefficients at the collector outside, radiation heat transfer coefficient at the collector plate surface and the convective heat transfer coefficient at between collector plate and the fluid (Chow, et al., 2009).

3 Method

The combined flat plate PVT liquid based collector and polycrystalline PV design used in this simulations is based on the unique PVT design currently in development by Solhybrid and explained in section 3.2.1.

3.1 Equipment

The only equipment necessary for this study is a computer since the study is fully based on the use of simulation software. The computer used is an HP running an Intel Core i7 CPU 2.80GHz, 8 GB RAM with windows 7 64-bit.

The thermal modeling is done using TAITherm 12.1.0, a finite volume based software that can provide a prediction of the full temperature distribution of a system. To solve for thermal conduction, radiation and convection TAITherm applies a multi-physics approach. (ThermoAnalytics, Inc, 2016)

3.2 Development of model

The model used in TAITherm is based on a PVT prototype which is currently under development by Solhybrid. The prototype is a glass-glass, parallel duct-type with either serial or parallel flow in the ducts.

First a thermal model is developed to represent the absorber attached on the back of the module using the graphical interface in TAITherm. There is no built in electrical model for PV cells, therefore the single diode model is implemented using the built in QT script tool to calculate the electrical power output. Temperatures calculated in the thermal model are pulled into the electrical model, and the resulting electrical production returned as a negative heat rate. As the computation needed for calculating the IV-curve uses a high amount of iterations, the accuracy will become a trade-off to the available computational power.

3.2.1 Thermal model

To maintain the simplicity, the thermal model is developed so that each cell of the mesh represents one cell of the PV module. A higher resolution is assumed to be redundant since only a single average temperature of the cell is used in determining electrical output. Additionally, temperature gradients within one cell are negligible because of the use of rectangular shaped ducts that cover the entire cell area. The PV is built into this cell as several conductive layers representing, glass, EVA, silicon, EVA and glass. The properties of each layer are presented in Table 3. Behind it, the duct is attached for the coolant using the properties of aluminium as the frame and water as the fluid properties according to Figure 9. A unique feature of this module is that the working fluid comes in direct contact with the PV module glass, rather than being completely contained by an extruded duct.

Figure 9 The PVT shown in layers as A: glass, B: EVA, C: PV cell, D: EVA, E: glass, F: aluminum frame and G: fluid.

The model is then constructed with 60 PV cells arranged in a six by ten array with either parallel flow as seen in Figure 10 or serial flow as in Figure 11. The flow through the PVT will create a temperature gradient along the duct and cause the PV cells to operate at different temperatures visualized with change in colour in Figure 8 and Figure 10. The working fluid is simulated with a 1-D flow model built into the TAITherm which uses mass flow rate as input and calculates the convective heat transfer coefficient using equivalent hydraulic diameters.

The flowrate used in previous studies is normally about 1-1.5 l per minute per m^2 (Calise, et al., 2012) (Haurant, et al., 2015). Although according to Duffie and Beckman (2013), modern solar thermal systems tend to use lower rates (0.12-0.36 l per minute and m^2) in order to maintain better stratification in the storage tank. In this study the flowrate will be evaluated from 0.06 to 0.79 l per minute per m^2.

The properties of the PV-module are based on the Perlight PLM-260P-60DG 270W and presented in Table 3 which has a rated efficiency at STC (standard test conditions, 1000 W/m^2 irradiance, AM1.5 spectrum and 25°C cell temperature) of 16.42% (Perlight Solar Co., Ltd, 2016).

Table 3 Properties used for the PV-module (ENF Ltd., 2016), (Armstrong & Hurley, 2010), (Perlight Solar Co., Ltd, 2016), (Fraunhofer Institute for Solar Energy, 2015), (Ioffe Physico-Technical Institute, 2001)

Layer	Thickness (mm)	Conductivity (W/(m*K))	Other
Front glass	2.5	0.81	AR coating, high transmittance, emissivity 0.95 & absorption 0.95.
Front EVA	0.45	0.34	Transparent, same optical properties as glass
PV silicon wafer	0.175	~149	
Back EVA	0.45	0.34	White
Back glass	2.5	1.1717	

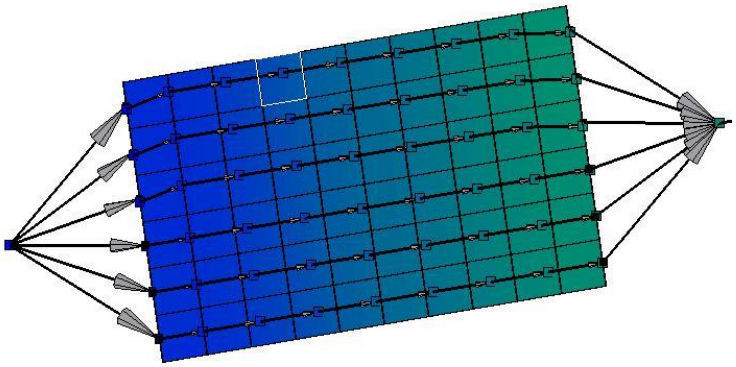

Figure 10 The parallel flow PVT model in TAITherm

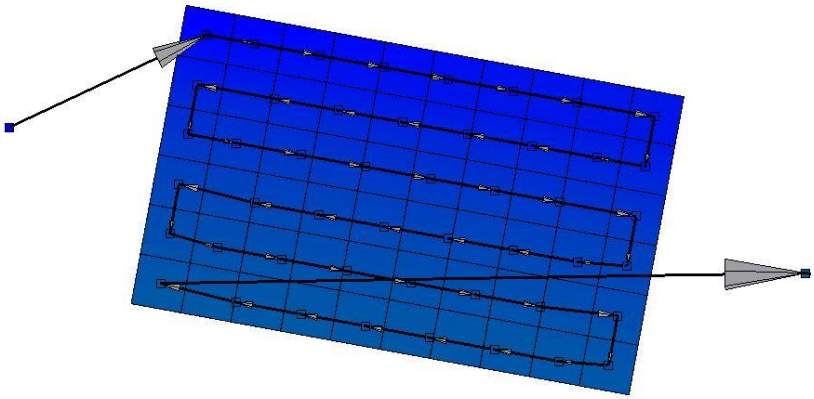

Figure 11 The serial flow PVT model in TAITherm

In order to represent the PV-module in TAITherm the two top layers, glass and transparent EVA, had to be removed and are instead handled with a modification to the convective heat transfer. This modification is done because TAITherm cannot simulate the two top layers as transparent meanwhile the rest where solid. Neither could the transparent layers be represented as a separate part with conduction between them and the silicon.

The modification is calculated as a ratio (C_R) for each wind speed using equation (16) where C_1 and C_2 are the two standard coefficients of the McAdams model used in TAITherm for calculating the convection coefficient, which are 5.7 and 3.8 respectively. V_w is the given wind speed, B_1 and k_1 are the thickness and conduction coefficients of the first layer, B_2 and k_2 are the thickness and conduction coefficients of the second. This ratio (C_R), seen in Table 4, is then implemented as an area multiplier for the top surface instead of the physical presence (original) of the layers. The silicon absorptivity was also recalculated to represent the reflection of irradiation in the glass.

$$C_R = \frac{\left[(C_1 + C_2 \cdot V_w)^{-1} + \frac{B_1}{k_1} + \frac{B_2}{k_2}\right]^{-1}}{(C_1 + C_2 \cdot V_w)} \qquad (16)$$

Table 4 Ratios between "original" and "modified" front glass and EVA layer

Wind speed (m/s)	Modified (W/m^2)	Original (W/m^2)	Ratio (-)
0	5,7	5,56	0,98
1	9,5	9,11	0,96
2	13,3	12,55	0,94
3	17,1	15,88	0,93
4	20,9	19,11	0,91
5	24,7	22,23	0,90
6	28,5	25,27	0,89
7	32,3	28,21	0,87
8	36,1	31,06	0,86
9	39,9	33,83	0,85
10	43,7	36,53	0,84
11	47,5	39,15	0,82
12	51,3	41,69	0,81
13	55,1	44,17	0,80
14	58,9	46,58	0,79
15	62,7	48,92	0,78

3.2.2 Electrical model

The electrical model used is the single diode model as it is a more advanced and accurate model to describe the behavior of the PV cell according to the studies mentioned in section 2.1.2 and 2.1.3. The parameters used in the single diode model are determined using the model described by (Ghani, et al., 2016) and represents the PV module PLM-260P-60DG 270W. The final parameters used for the single diode model equation are presented in Table 5.

Table 5 Reference parameters (Ghani, et al., 2016).

Reference parameters	**Value**
$I_{O,ref}$	1.0888e-8
$I_{L,,ref}$	9.0507
R_s	0.004255
R_{sh}	56.052
n_I	1.2

3.2.3 Implementation of single diode model in TAITherm

In order to calculate the power output depending on a non-uniform temperature distribution, the equations in section 2.1.3 must be solved for every cell throughout the PVT module for every time step of the simulation. Moreover, the temperature of the cell is dependent on the power output which forces the solution to be determined iteratively. The implementation according to Figure 12 is done using QT script in the script editor built into TAITherm. The code is attached in Appendix A.

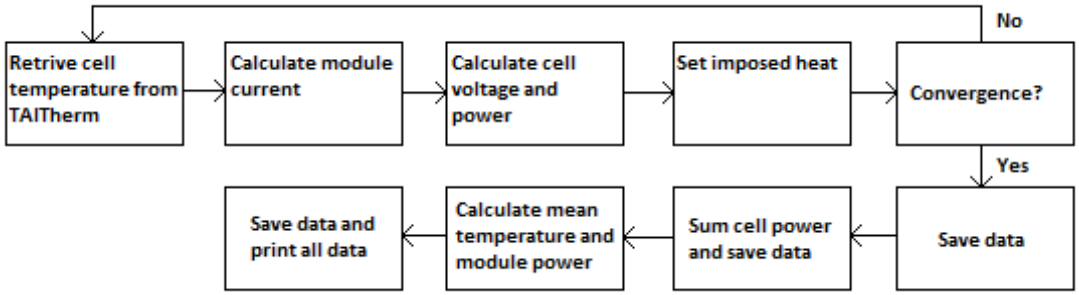

Figure 12 Flow chart of cell power detection

At the end of every thermal iteration TAITherm gives the cell temperature of each cell so that the current at maximum power point (I_{mp}) is calculated through determining the zero-derivative of equation (6) at the average temperature of all the PV cells. The current is then set as the module current so that the voltage and further on the power can be calculated for every cell based on the IV-curve given by equation (6) in section 2.1.3 at the temperature in every cell. The total power is then calculated as the sum of all cells for both the average temperature case and the non-uniform case for verification of the model.

3.3 Simulation

The simulation is done in steady state considering a range of flow rates, wind speeds, irradiances, convection coefficients for the working fluid and back surface, inlet temperatures and ambient temperatures on both a PVT with parallel and serial flow patterns. This is done in order to compare the impact of these parameters on the final power output by creating more than 50 scenarios. At the end of iteration the thermal power is calculated with equation (17)

$$\dot{Q}_{th} = \dot{m} C_p (T_{out} - T_{in}) \qquad (17)$$

4 Results

The difference between using a cell-resolution numerical simulation and a module-resolution numerical simulation shown in Figure 13 is small. Although, it can be seen in Figure 13 that the non-uniform temperature power curve is smoother than the uniform temperature power curve; despite this, the difference is small as it is close to one-hundreds of the total electrical power output per square meter. A similar tendency is seen across all simulations, therefore only the non-uniform temperature results are given in the remaining figures.

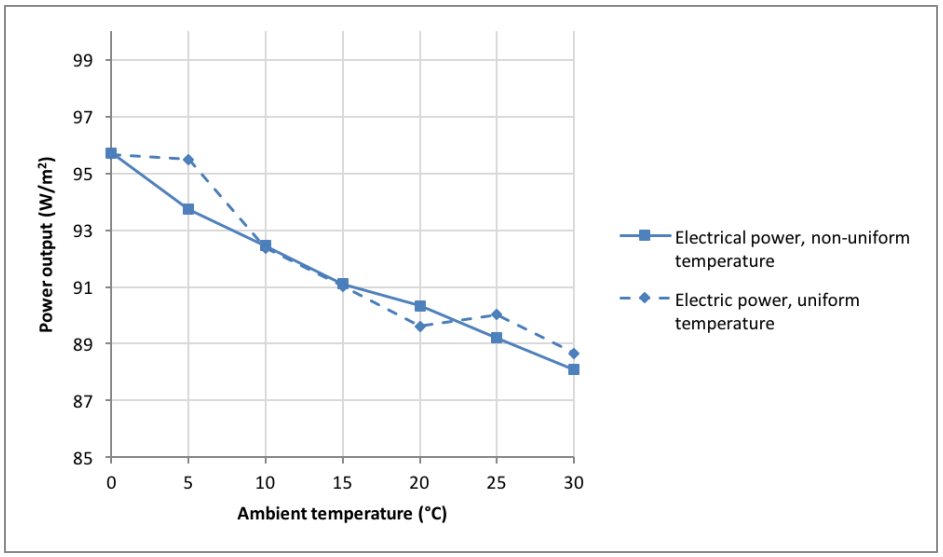

Figure 13 Difference in electrical flux between uniform and non-uniform temperature

The two flow patterns investigated show little or no difference in total power output as seen in Figure 14, therefore only simulations with serial flow will be presented in the results, but is representative for both cases.

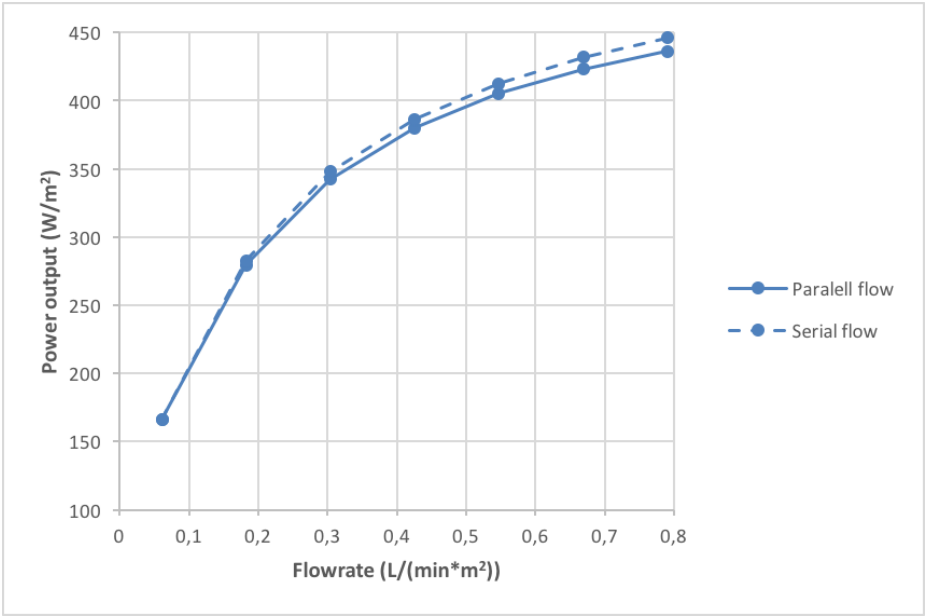

Figure 14 Difference in total flux depending on flow-pattern

All simulations have a standard case as presented in Table 6 together with the high and low values for possible scenarios. The simulations are done by varying one of the parameters in Table 6 at a time, while

the others are kept constant. The values of the parameters chosen in Table 6 are based on data from the review and (SMHI, 2013), where the irradiance, ambient temperature and wind speed represent values typically seen during the most productive solar months (April-September) in Stockholm, Sweden. The results are shown in Figure 15 to Figure 23 below.

Table 6 Parameters of the standard case

Parameter	Nominal	Low	High
Irradiance (W/m²)	600	100	900
Ambient temperature (°C)	15	0	30
Wind speed (m/s) (only on front)	5	0	12
Flowrate (l/min)	0.5	0.1	1.3
Inlet temperature (°C)	10	0	20

4.1 Variation of flowrate

The flowrate of the coolant through the heat absorber has a significant impact on the thermal power and a slight but noticeable impact on the electrical output as seen in Figure 15. This shows that the thermal output increases along with increased flowrate but flattens out at higher rates. A slight increase of five percent between 0.06 to 0.79 l/(min*m²) in electrical power can be seen, as the increased flowrate will decrease the average cell temperature. It can be stated that it is more beneficial to have a high flowrate both for the thermal and electrical power outputs, but it should be mentioned that an increased flowrate will increase power used by the circulation pump. However, the increased electrical power in a system of e.g. 10 modules will be about 75W according to figure 15 at 15°C between the lowest and the highest flowrate suggesting that it should be more than enough to motivate a higher flowrate when examining the difference between highest and lowest power used by two pumps, Wilo Star S 16 F (http://www.wilo-canada.com) and Taco HEC-2 (http://www.taco-hvac.com). Although, as seen in Figure 15, the curves are flattened out for all three of the ambient temperature cases as the flowrate increases which shows that the benefit of increasing the flowrate will decrease in higher regions. The system behaves similar for the different ambient conditions but it can be stated generally that the higher the ambient temperature is, the higher the thermal power will be and the lower the electrical power will be.
The outlet temperature must be considered when choosing the flowrate depending on the design of the system the PVT is connected to as heat pumps will not allow too high or too low temperatures. Outlet temperatures, for the simulations with an ambient temperature of 5°C, where recorded in the range 16.1 to 49.7°C as the flowrate was decreased from 0.79 to 0.06 l/(min*m²).

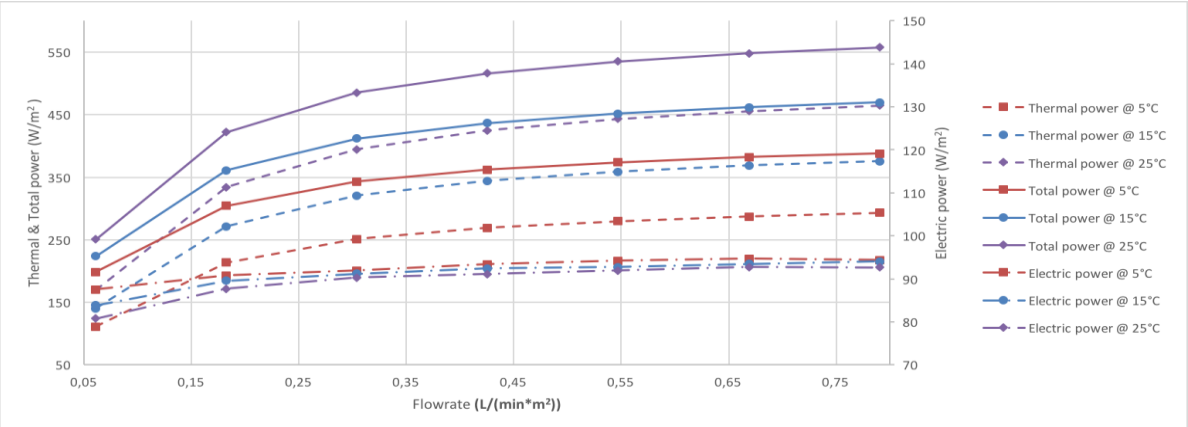

Figure 15 Total, thermal and electrical flux as a function of flowrate at three ambient temperatures

4.2 Variation of irradiation

As the irradiation increases, both the electrical and thermal power output will increase significantly as seen in Figure 16. Although, it can be seen that the thermal output at 100 W/m² of irradiance in the diagram in Figure 16 is higher than the expected, this is caused by the system also extracting energy from the ambient air which in these simulations is set to 15 °C. The total increase in electrical power is 828 percent when the irradiance is increased from 100-900 W/m² (800 percent increase). Although the module efficiency at 100W/m² irradiation is 81 percent, 59 percent at 500 W/m² and 56 percent at 900W/m², showing that the module is highly effective when the majority of energy is extracted from the environment but drops the irradiance becomes stronger. When comparing the difference in efficiency between 100W/m² and 500W/m² with the difference between 500W/m² and 900W/m² it can be seen that the efficiency stabilizes as the irradiance becomes stronger.

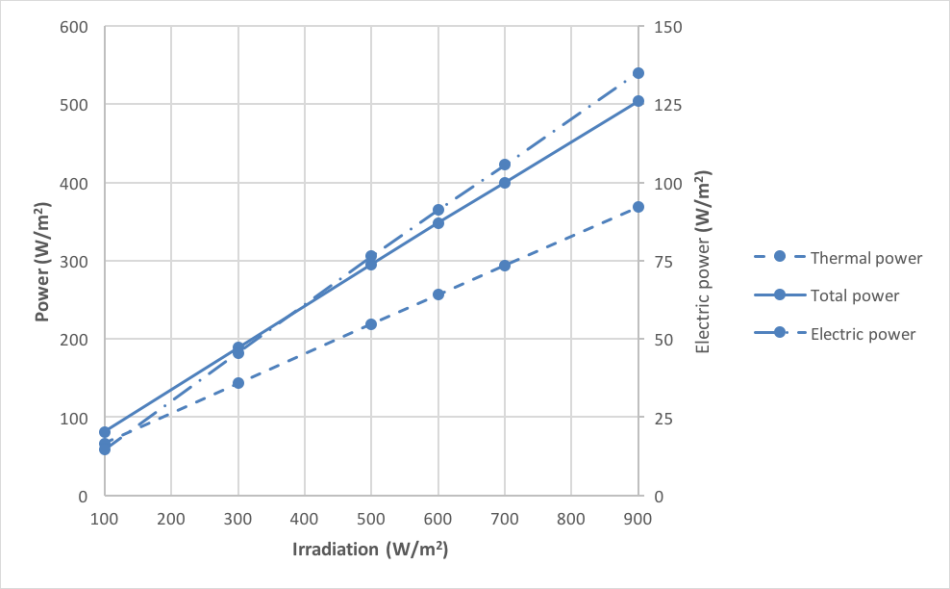

Figure 16 Total, thermal and electrical flux as a function of irradiation

4.3 Variation of ambient temperature

Variation in the ambient temperature has the most impact on the thermal power output as the energy added or subtracted from the system is highly dependent on the convective heat transfer. The irradiation in Figure 17 is set to 600 W/m² while the total energy output ranges from 160-540 W/m² for the corresponding temperature range of 0-30°C at 10°C inlet fluid temperature. This is equivalent to an increase of 600 percent for the thermal output while the electrical output decreases by 8 percent (95.8W/m²-88.2W/m²). Figure 17 also shows the 5°C and 15°C inlet fluid temperature for comparison reasons, the nominal increase in power from 15°C to 10°C inlet fluid temperature is 75 percent and from 10°C to 15°C inlet fluid temperature is 41 percent. In the 15°C inlet simulation the thermal power at low ambient temperatures becomes barely below zero (-4W/m²). On the other hand, the low inlet temperature helps to improve the cold weather performance as the mean temperature of the module can be held at lower temperatures.

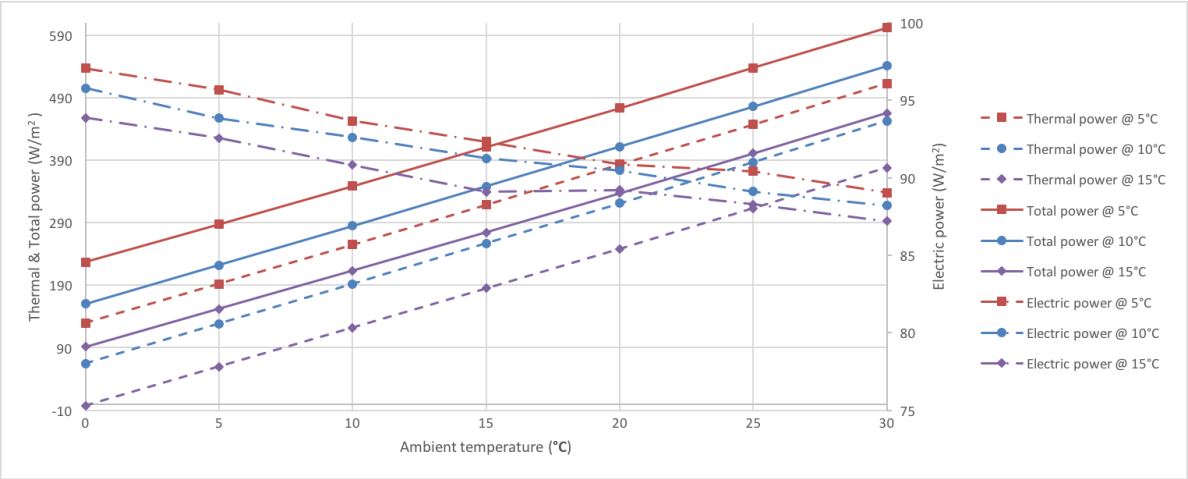

Figure 17 Total, thermal and electrical flux as a function of inlet and ambient temperatures

4.4 Variation of wind speed

The increased wind speed will reduce the thermal power output even though the ambient air is higher than the inlet temperature of the heat absorber as seen in Figure 18. This is due to the irradiation increasing the mean temperature of the PVT above the ambient temperature resulting in a net convective loss. The electrical power on the other hand increases with 2.6 percent (90.4-92.8 W/m²) in the range 0-12 m/s while the thermal power decreases by 44.3 percent (405.8-268.5 W/m²).

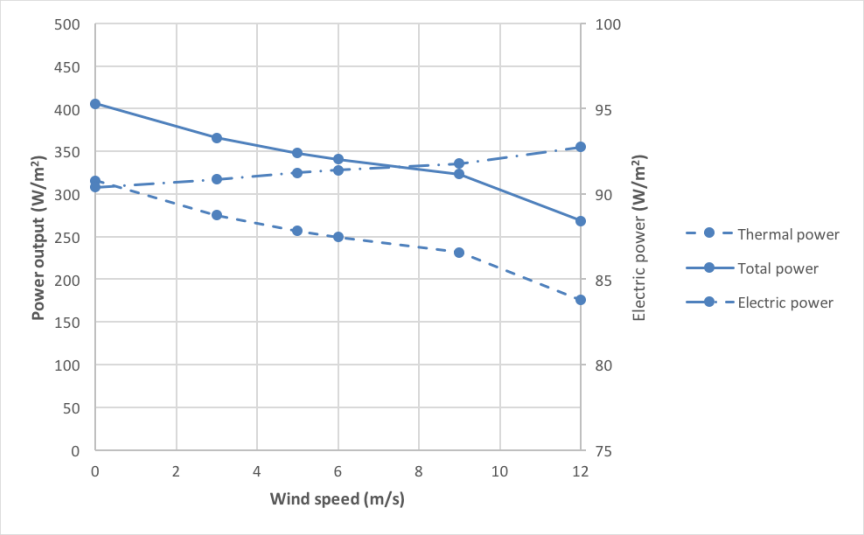

Figure 18 Total, thermal and electrical flux as a function of wind speed

4.5 Variation of internal convection

When changing the convection coefficients related to coolant, flow it can be seen in Figure 19 that the impact is small. The increase from the left to the right of the curve is 5.6 percent for the thermal power and 0.5 percent for the electrical power. This variation is much lower than expected and may be a drawback of using a 1-D model for simulating the flow. A fully 3-D computer fluid dynamic model would probably have shown a different result. As the conductive heat transfer between the fluid and the duct is almost negligible, all flux should be through convection and moreover be more dependent on the change of conduction in TAITherm, e.g. a decrease of 40 percent should decrease the flux by the same.

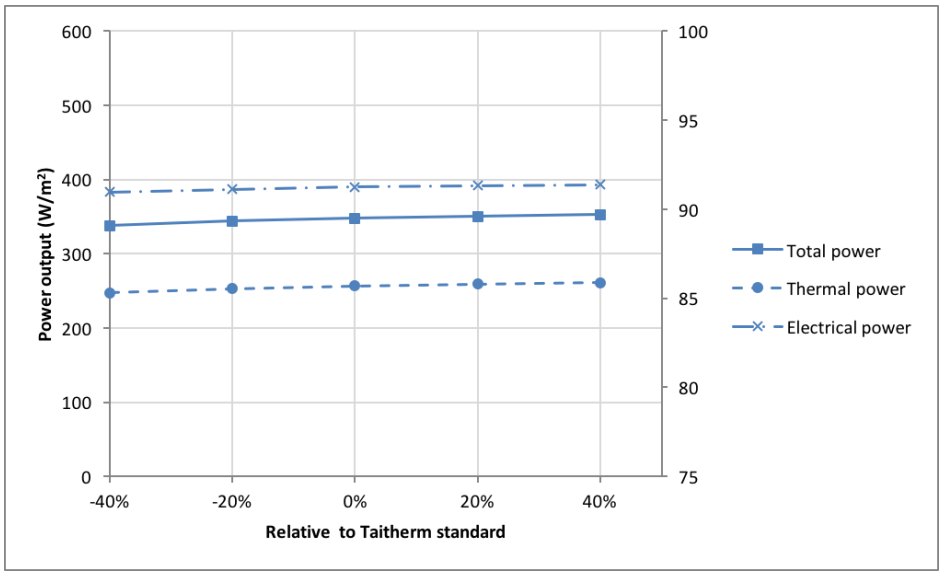

Figure 19 Total, thermal and electrical flux as a function of convection in flow

4.6 Variation of convection on back

Since there is a notable uncertainty about the ability of wind to flow underneath the backside of the modules, a range of convection coefficients are checked. The nominal condition used in the other sensitivity studies have no convection off the rear side, meaning that the zero percent case in the rear convection is the same as the 5 m/s wind speed case. At 100 percent, the wind passing over the rear of the module is equal to the wind passing over the front, and just the convection coefficients are the same. Comparing the wind sensitivity results shown in Figure 18 to the rear convection sensitivity results shown in Figure 20, it can be seen that power output differences caused by wind speed are higher than from changing the convection on the back. This may be surprising given the considerable increase in convective potential, as shown in Table 7. However, the rear temperature of the collector is much lower than the front which reduces the total convective heat rate, particularly when the average working fluid temperature is close to ambient.

Table 7 Variation of convection coefficients tested on the back of the collector

	3 m/s, 0%	5 m/s, 0%	5 m/s, 100%
Front (W/m²*K)	15.88	22.23	22.23
Back (W/m²*K)	0	0	22.23

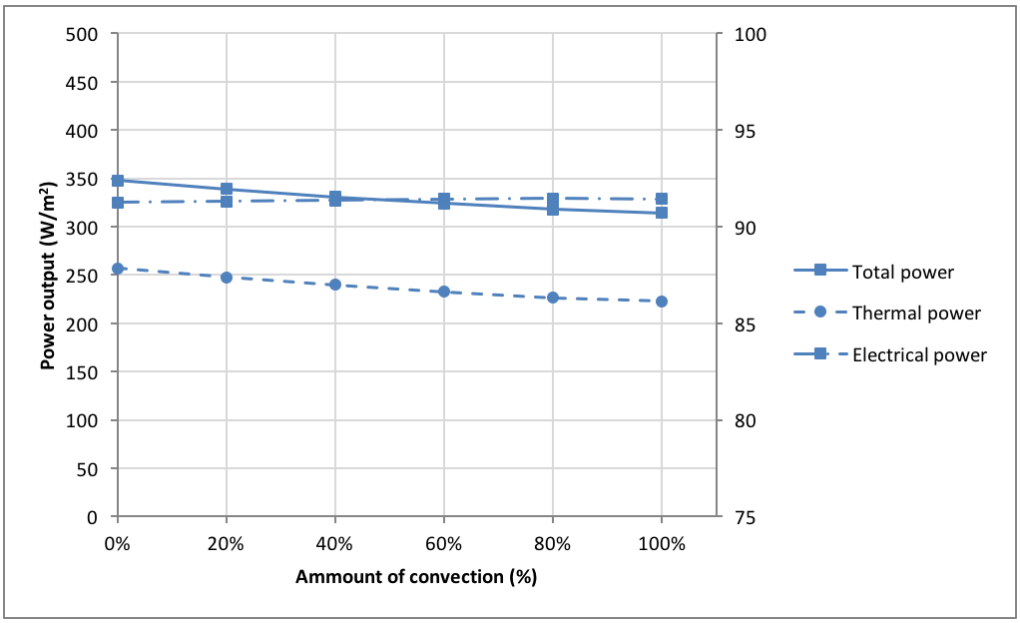

Figure 20 Relative amount of convection on the back of the PVT

4.7 Variation of inlet temperature

The variation of the inlet temperature shows an inverse relationship where the power output decreases along with increasing temperature. This is expected since there is a greater potential for heat gains from the ambient when the temperature difference is negative. As shown in Table 6, the ambient temperature in the standard case is set to 15 °C which means the inlet temperature will be 5 °C higher in the far right of the diagram in Figure 21

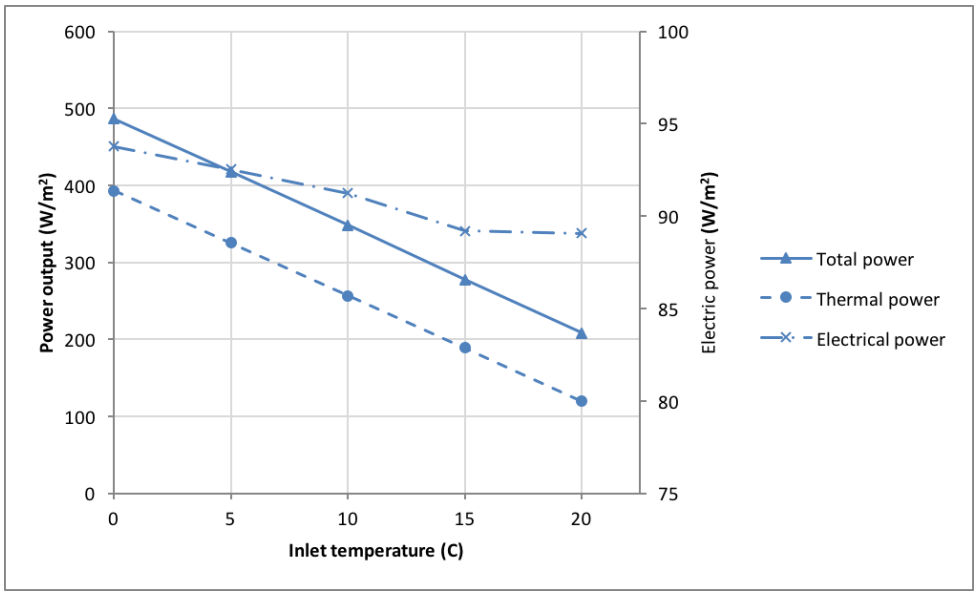

Figure 21 Total, thermal and electrical flux as a function of the inlet temperature

4.8 Sensitivity analysis

When comparing the sensitivity of all the parameters in Figure 22 it can be seen that the irradiance has the highest impact on the total power output followed by the ambient temperature. Both of these are of course not a design matter as compared to the rest of the parameters investigated, excluding for wind speed. The second two most important parameters are the flowrate and the inlet temperature. The increased inlet temperature will, as mentioned before, decrease both the thermal and electrical power output due to losses

with the ambient air. On the other hand it will increase efficiency as the temperature of the inlet decreases since heat is being extracted from the air. This suggests that the inlet temperature should be as low as possible. It must though be mentioned that when the temperature on the PVT decreases too much as compared to the ambient that there could be condensation on the front glass surface that would interfere with the absorbed irradiance, which is not captured in these results.

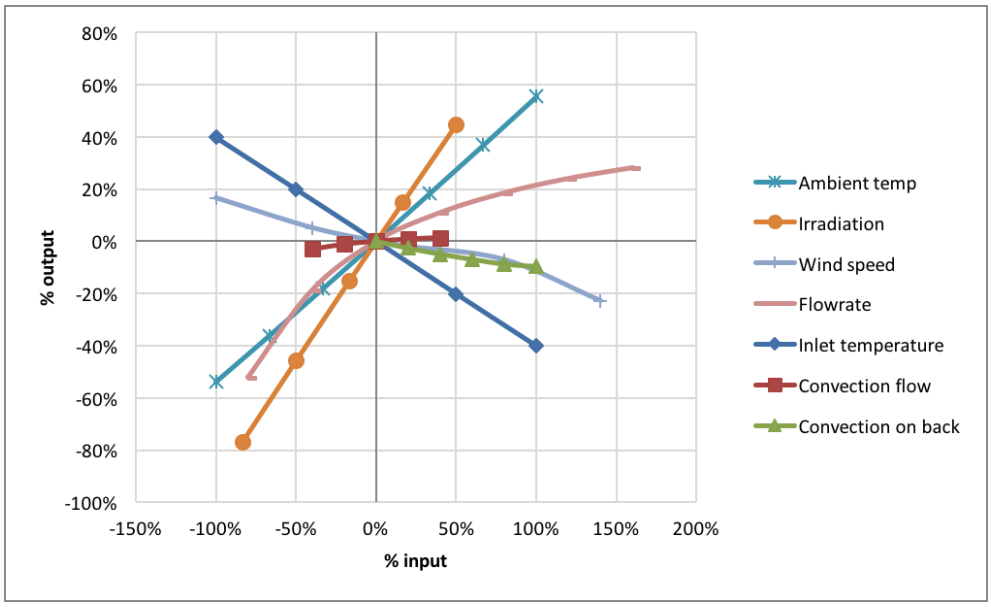

Figure 22 Sensitivity results considering primary boundary conditions on total flux

Figure 23 shows the efficiency as a function of irradiance and the temperature difference between the average module temperature and the ambient temperature. The intersection between all the curves is the standard case where the ambient temperature still is higher than the mean temperature of coolant in the PVT. When compared to a previous study of a glazed and insulated collector by Dupeyrat, et al (2011), shown in Figure 24, it can be seen that the optical efficiency (the efficiency when at the y-axis intercept) is approximately 10% lower. Unglazed collectors can be characterized by their much lower efficiency as inlet temperatures rise above the ambient. This can be seen by comparing the slope of the dark blue curve in Figure 23 to the MPP curve in Figure 24. Conversely, when the mean temperature of the coolant is lower

than the ambient, as can be the case much of the time with a GSHP system, the collector will gain heat from the ambient air and increase the efficiency over a glazed collector.

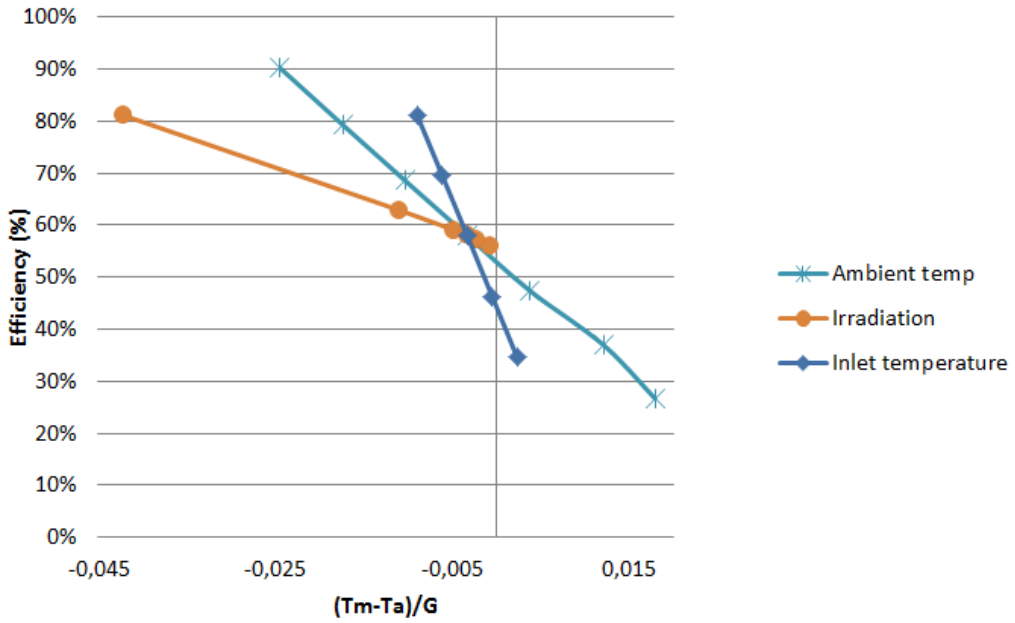

Figure 23 Efficiency compared to the reduced temperature

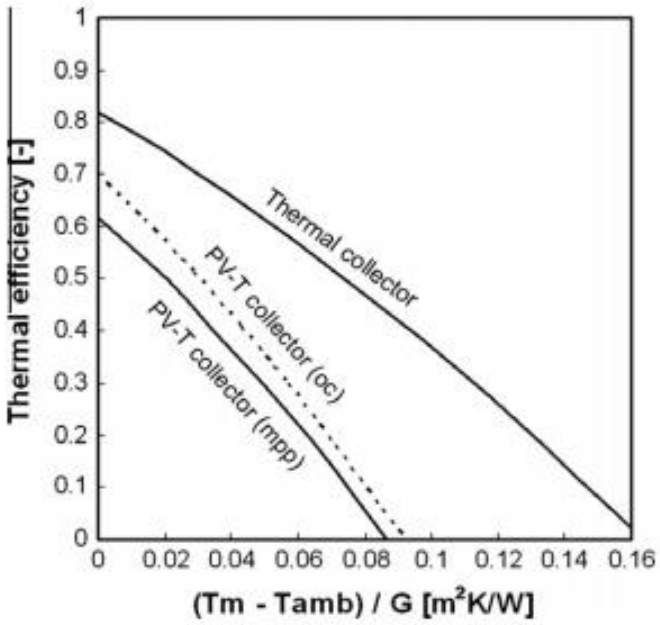

Figure 24 Efficiency compare to the reduced temperature (Dupeyrat, et al., 2011)

5 Discussion and Conclusion

Pressure drop for each collector design is not determined in this study since it is not considered to have a significant impact on the module power output. However, it must be considered at a systems level since the power used by the circulation pump is dependent on it.

As the study shows that the difference between uniform and non-uniform is little or negligible together with the simulation becoming highly time demanding, 10-20 minutes per time step, the cell-resolution numerical method is redundant. However, the time for simulation can be reduced by implementing an optimization model for the numerical method.

The flowrate through the module can be observed to have a major impact on the thermal output, this information however, comes with an uncertainty built into the model as the software used only simulates a 1-dimensional flow. 1D flow models can be accurate but can be limited in a complicated flow pattern and heat transfer problems such as this. The next step would be to perform an in depth CFD simulation. This report presents how the flowrate changes the power output but not the precise flowrate to use in a final design, which will depend on the system which the collector is used in. However, choosing as high flowrate as possible is recommended.

The impact of the ambient temperature can be reduced by implementing some kind of insulation, especially on the back where it will not decrease the irradiation that hits the PV-cell. However this is something that needs to be decided depending on the usage of the PVT. If the main purpose of the system is to be run during the summer in order to decrease the temperature of the PV and to provide the GSHP system with heat to charge the borehole, the insulation can be a hindrance to capturing energy from the ambient air. On the other hand, the insulation can allow for the PVT to provide heat earlier at the year and replace the need of the GSHP system extracting heat from the ground at an earlier stage.

The influence of the wind on the front surface has a significant impact on the thermal power output as expected. The decrease in thermal power; brings the question back to mind about if the PVT should have an extra pane of glass insulating the front from the wind. Like rear insulation, front insulation would reduce the gains from the ambient air, as well as expose the collector to the risk of condensation forming inside the casing and causing damage.

The inlet temperature has the most significant impact on the thermal power output as a high inlet temperature will reduce the thermal power heavily. Although when the inlet temperature instead is decreased, both the thermal power and the electrical power will increase. A low inlet temperature is therefore recommended if kept in mind risks of changes in the power outputs due to condensation or freezing.

The non-uniform temperature distribution throughout the cells does not impose the need for a cell-resolution numerical method in the system modelling; this is due to the difference between the cell-resolution and the mean temperature calculation of the power output being little or negligible and also the process being time-demanding. Although this is dependent on the system being limited to using just one PVT. For systems of more than one PVT further investigation is needed.

At the time of publication, a physical prototype of the collector had not yet been completed. Future work should include validating the model with empirical data.

6 Bibliography

Akhatov, J. S., Avezov, R. R. & Avezova, N. R., 2011. A review on Photovoltaic-Thermal (PV-T) Air and Warer Collectors. *Applied Solar Energy,* 47(3), pp. 169-183.

Armstrong, S. & Hurley, W. G., 2010. A thermal model for photovoltaic panels under varying atmospheric conditions. *Applied Thermal Engineering,* Volume 30, pp. 1488-1495.

Bakker, M. et al., 2003. Performance and costs of a roof-sized PV/thermal array combined with a ground coupled heat pump. *Solar Energy,* 78(2), pp. 331-339.

Calise, F., Dentice d'Accadia, M. & Vanoli, L., 2012. Design and dynamic simulation of a nocel solar trigeneration system based on hybrid photovoltaic/thermal collectors (PVT). *Energy Conversion and Management,* Volume 60, pp. 215-225.

Charalambous, P. G., Maidment, G. G., Kalogirou, S. A. & Yiakoumetti, K., 2007. Photovoltaic thermal (PV/T) collectors: A review. *Applied Thermal Engineering,* Volume 27, pp. 275-286.

Chow, T. T., 2003. Performance Analysis of Photovoltaic-Thermal collector by explicit dynamic model. *Solar Energy,* Volume 75, pp. 143-152.

Chow, T. T., 2009. A review on photovoltaic/thermal hybrid solar technology. *Applied Energy,* Volume 87, pp. 365-379.

Chow, T. T. et al., 2008. Computer modeling and experimental validation of a building-integrated photovoltaic and water heating system. *Applied Thermal Engineering,* 28(11-12), p. 1356–1364.

Chow, T. T., He, W. & Ji, J., 2006. Hybrid photovoltaic-thermosyphon water heating system for residential application. *Solar Energy,* 80(3), pp. 298-306.

Chow, T. T. et al., 2009. Energy and exergy analysis of photovoltaic-thermal collector with and without glass cover. *Applied Energy,* Volume 86, pp. 310-316.

Daghigh, R., Ruslan, M. H. & Sopian, K., 2011. Advances in liquid based photovoltiac/thermal (PV/T) collectors. *Renewable and Sustainable Energy Reviews,* Volume 15, pp. 4156-4170.

Dalvand, M. J., Mohtasebi, S. S. & Rafiee, S., 2012. A technical study on hybrid photovoltaic/thermal solar collectors. *Elixir Agriculture,* Volume 47, pp. 8999-9004.

De Soto, W., 2004. *Improvement and Validation of a Model for Photovoltaic Array Performance,* Wisconsin-Madison: Solar Energy Laboratory University of Wisconsin-Madison.

del Pero, C., Aste, N. & Leonforte, F., 2014. Water flat plate PV-thermal collectors: A review. *Solar Energy,* Volume 102, pp. 98-115.

Dubey, S., Sarvaiya, J. N. & Seshadri, B., 2013. Temperature Dependent Photovoltaic (PV) Efficiency and Its Effect on PV Production in the World - A Review. *Energy Procedia,* Volume 33, pp. 311-321.

Duffie, J. A. & Beckman, W. A., 2013. *Solar Thermal Power Systems.* 4 ed. Wisconsin-Madison: John Wiley & Sons, Inc..

Dupeyrat, P., Ménézo, C., Rommel, M. & Henning, H.-M., 2011. Efficient single glazed flat plate photovoltaic–thermal hybrid. *Solar Energy,* Volume 85, pp. 1457-1468.

Energimyndigheten, 2016. *Solceller.* [Online] Available at: http://www.energimyndigheten.se/fornybart/solenergi/solceller/ [Accessed 19 07 2016].

ENF Ltd., 2016. *Solar Panel EVA Directory.* [Online] Available at: http://www.enfsolar.com/pv/eva [Accessed 30 05 2016].

European Commission, 2016. *Paris Agreement.* [Online] Available at: http://ec.europa.eu/clima/policies/international/negotiations/paris/index_en.htm [Accessed 21 03 2016].

Fraisse, G., Ménézo, C. & Johannes, K., 2007. Energy performance of water hybrid PV/T collectors applied to combisystems of Direct Solar Floor type. *Solar Energy,* 81(11), pp. 1426-1438.

Fraunhofer Institute for Solar Energy, 2015. *Fraunhofer.* [Online] Available at: https://www.ise.fraunhofer.de/de/downloads/pdf-files/aktuelles/photovoltaics-report-in-englischer-sprache.pdf
[Accessed 30 05 2016].

Fujisawa, T. & Tatsuo, T., 1997. Annual exergy evaluation on photovoltaic-thermal hybrid collector. *Solar Energy Materials and Solar Cells,* Volume 47, pp. 135-148.

Ghani, D., Rosengarten, G. & Duke, M., 2016. The characterisation of crystalline silicon photovoltaic devices using. *Solar Energy,* Volume 132, pp. 15-20.

Gómez, G. C., 2009. *Heat transfer in a photovoltaic panel,* Lund: Lund University.

Green, M. A., 1982. *Solar Cells: operating principles, technology and system applications.* s.l.:Englewood Cliffs, N. J. : Prentice-Hall.

Haurant, P., Menezo, C., Gaillard, L. & Dupeyrat, P., 2014. Dynamic numerical model of a high efficiency PV–T collector integrated into a domestic hot water system. *Solar Energy ,* Issue 111, pp. 68-81.

Haurant, P., Ménézo, C., Gaillard, L. & Dupeyrat, P., 2015. Dynamic numerical model of a high efficiency PV–T collector. *Solar Energy,* Volume 111, pp. 68-81.

Holman, J. P., 2009. *Heat Transfer.* 10 International Edition ed. s.l.:McGraw Hill Higher Education.

Huang, B. J., Lin, T. H., Hung, W. C. & Sun, F. S., 2001. Performance evaluation of solar photovoltaic/thermal systems. *Solar Energy,* 70(5), pp. 443-448.

Ioffe Physico-Technical Institute, 2001. *Thermal properties.* [Online] Available at: http://www.ioffe.ru/SVA/NSM/Semicond/Si/thermal.html [Accessed 30 05 2016].

Ito, S., Miura, N. & Takano, Y., 2005. *Studies of Heat Pumps Using Direct Expansion Type Solar Collectors,* Atsugi: Department of System Engineering, Kanagawa Institute of Technology.

Jee, M. J., Iniyan, S. & Ranko, G., 2015. Flat plate solar photovoltaic–thermal (PV/T) systems: A reference guide. *Renewable and Sustainable Energy Reviews,* Volume 51, pp. 62-68.

Ji, J. et al., 2007. Thermal analysis of PV/T evaporator of a solar-assisted. *INTERNATIONAL JOURNAL OF ENERGY RESEARCH,* Volume 31, pp. 525-545.

Ji, J. et al., 2007. A sensitivity study of a hybrid photovoltaic/thermal water-heating system with natural circulation. *Applied Energy,* Volume 84, pp. 222-237.

Keilang, L. et al., 2009. Performance study of a photovoltaic solar assisted heat pump. *Renewable Energy,* Volume 34, pp. 2680-2687.

Kemmoku, Y. et al., 2004. *Modelling of Module Temperature of a Concentrator PV System,* s.l.: EU PVSEC.

makeitfrom.com, 2015. *Ethylene Vinyl Acetate (EVA).* [Online] Available at: http://www.makeitfrom.com/material-properties/Ethylene-Vinyl-Acetate-EVA/ [Accessed 29 02 2016].

Perlight Solar Co., Ltd, 2016. *Perlight Solar.* [Online] Available at: http://perlight.com/products_show.asp?cateid=36 [Accessed 06 06 2016].

Polysciences, Inc., 2015. *Poly(ethylene/vinyl acetate) [60:40 (wt)]*. [Online] Available at: http://www.polysciences.com/default/catalog-products/monomers-polymers/polymers/poly-eva-poly-evoh/polyethylenevinyl-acetate-6040-wt/ [Accessed 29 02 2016].

Robles-Ocampo, B. et al., 2007. Photovoltaic/thermal solar hybrid system with bifacial PV module and transparent plane collector. *Solar Energu Materials & Solar Cells,* Volume 91, pp. 1966-1971.

Sandnes, B. & Rekstad, J., 2002. A Photovoltaic/Thermal (PV/T) Collector with Polymer Absorber Plate. Experimental Study and Analytical Model. *Solar Energy,* 1(72), pp. 63-73.

Santbergen, R., 2008. *Optical Absorption Factor of Solar Cells for PVT Systems,* Eindhoven: Technische Universiteit Eindhoven.

Santbergen, R., Goud, J. M. & van Zolingen, R. J., 2007. *An optical model for the absorption factor of thin-film photovoltaic cells,* Eindhoven: Eindhoven University of Technology.

Santbergen, R., Rindt, C. C., Zondag, H. A. & van Zolingen, R. J., 2010. Detailed analysis of the energy yield of system with covered sheet-and-tube PVT collectors. *Solar Energy,* Volume 84, pp. 867-878.

Santbergen, R. & van Zolingen, R. J., 2008. The absorption factor of crystalline silicon PV cells: A numerical and experimental study. *Solar Energy Materials & Solar Cells,* Volume 92, pp. 432-444.

SMHI, 2013. *Solinstrålning.* [Online] Available at: http://www.smhi.se/kunskapsbanken/meteorologi/solstralning-1.4186 [Accessed 11 03 2016].

SMHI, 2015. *Solstrålning i Sverige.* [Online] Available at: http://www.smhi.se/kunskapsbanken/meteorologi/solstralning-i-sverige-1.89984 [Accessed 31 05 2016].

ThermoAnalytics, Inc, 2016. *ThermoAnalytics.* [Online] Available at: http://www.thermoanalytics.com/products/taitherm

Tiwari, A., Sodha, M. S., Chandra, A. & Joshi, J. C., 2006. Performance evaluation of photovoltaic thermal solar air collector for composite climate of India. *Solar Energy Materials and Solar Cells,* 90(2), pp. 175-189.

Tiwari, G. N., Mishra, R. K. & Solanki, S. C., 2011. Photovoltaic modules and their applications: A review on thermal modelling. *Applied Energy,* Volume 88, pp. 2287-2304.

Tripanagnostopoulos, Y., Nousia, T., Souliotis, M. & Yianoulis, P., 2002. Hybrid photovoltaic/thermal solar systems. *Solar Energy,* 72(3), pp. 217-234.

Willeke, G. P. & Weber, E. R., 2015. *Advances in Photovoltaics: Part 4*. Freiburg: Academic Press is an imprint of Elsevier.

Zondag, H. A., 2008. Flat-plate PV-Thermal collectors and systems: A review. *Renewable and Sustainable Energy Reviews,* Volume 12, pp. 891-959.

Zondag, H. A. et al., 2002. The thermal and electrical yield of a PV-thermal collector. *Solar Energy,* 72(2), pp. 113-128.

Zondag, H. A. et al., 2003. The yield of different combined PV-thermal collector designs. *Solar Energy,* 74(3), pp. 253-269.

7 Appendix A

```
function retrievenodetempNEW(userString)//-----------------------
                //This function return the temperature of the input element number
{
  var api = new API;
   // Retrieves the FRONT SURFACE temperature of the element
   var elemNodeIdx = new ReturnValueInt;
   var sensorElemIdx = new ReturnValueInt;
   var sensorElem = userString;
   var temp
                var status = api.getElementIndex(sensorElem, sensorElemIdx);
                if (status != api.success) api.abortSolutionWithMessage("Invalid Element ID " +
sensorElem);
                status = api.elementSurfaceNode( sensorElemIdx.value, api.front, elemNodeIdx );
                if (status == api.success) {
                   var nodeTemp = new ReturnValueDouble;
                   status = api.getTemperature( elemNodeIdx.value, nodeTemp );
                   if (status == api.success)
                                temp = nodeTemp.value - 273.15;
                   else
                                System.println( "Failed to retreieve temperature of node " +
elemNodeIdx.value );
                }
                else {
                   System.println( "Failed to retrieve the temperature of element " + sensorElem );
                }
                return temp
   }



function CalculateAverageTemp()//-----------------------------------
{
   var sensorElem = 0;
   var sumTemp=0;
   var numberOfCells = 0;
```

```
   for (var j = 0; j<=5;j++)// this for-loop enables to iterate thru all front pv-cells
   {
                  var AA=elements[j*2];
                  var BB=elements[j*2+1];
                  for (var i = AA; i<=BB; i++)
                  {
                     sensorElem =  i;
// Har ska jag berakna medeltemperaturen genom att summera alla temperaturer
                     numberOfCells=numberOfCells +  1;
                     sumTemp = sumTemp +retrievenodetempNEW(sensorElem);
                  }
   }
   averageTemp = sumTemp/numberOfCells;
}


function retrieveirradiation() //------------------------
{
   var api = new API;
   var elemNodeIdx = new ReturnValueInt;
   var sensorElemIdx = new ReturnValueInt;
   var sensorElem = 10;

   var status = api.getElementIndex(sensorElem, sensorElemIdx);
   if (status != api.success) api.abortSolutionWithMessage("Invalid Element ID " + sensorElem);

   status = api.elementSurfaceNode( sensorElemIdx.value, api.front, elemNodeIdx );

   if (status == api.success) {
                  var nodeIRRAD = new ReturnValueDouble;
                  status = api.getTotalSolar(nodeIRRAD );
                  if (status == api.success)
                     IRRAD = nodeIRRAD.value;
                  else
                     System.println( "Failed to retreieve temperature of node " + elemNodeIdx.value );
   }
```

```
   else {
                System.println( "Failed to retrieve the temperature of element " + sensorElem );
   }

   S_Sref=IRRAD/Gref;

}


function calculateImp() //------------------------------
{

   //Average cell temperature
   var t_c = averageTemp+273.15;

   // calculating the Imp to be used for furter power calculations

   var  a = N_s*n_I*k*t_c/q;
   var  I_L = S_Sref*(I_L_ref+alpha_Isc*(t_c-T_C_ref)); //eq 11
   var E_g_Tc = E_g_tref*(1-0.0003174*(t_c-T_C_ref)); // Duffie & Beckman
   var I_O = I_O_ref*((t_c/T_C_ref)^3)*Math.exp((1/k)*(E_g_tref/T_C_ref-E_g_Tc/t_c));// Duffie &
Beckman

   var Pnew=0.000001;
   var Pold=0;
   var I;
   var v = 0.1;
   while ((Pnew>Pold))
   {
                v=v+0.01;
                I = 0;
                var error = 5;
                while ((Math.abs(error) > 0.01) && (Math.abs(error)<100))
                {
                   I = I + 0.001;
                   error = I_L - I_O*(Math.exp((v+I*R_S)/a)-1)-(v+I*R_S)/R_SH - I; //eq 1
```

```
                }
                if (Math.abs(error)>100)
                {
                   System.print(" **Error too large" + error + " first    I: " + I +"V: " + v + "Io: " + I_O);
                }

                Pold=Pnew;
                Pnew=I*v;

   }
   PaverageTemp=Pnew*60;
   Imp=I;
}

function calculateP() //------------------------------
{
   // Define constants

   var SaveCellPower =[];
   // Calculate power of each cell-----------------------------------------------------------------------------------
-
// This is done for every iteration since the power output will decrease the heat applied to the absorber
   //It also sets the imposed heat for the cell
   var api = new API;
   var sensorElem = 0;
   var elementTemp=0;
   var numberOfCells = 0;
   var totalPower = 0;
    //11-180

   for (var j = 0; j<=5;j++) // this for-loop enables to iterate thru all front pv-cells
   {
                var AA=elements[j*2];
                var BB=elements[j*2+1];
                var PendIter = 0;
                for (var i = AA; i<=BB; i++)
```

```
{
    sensorElem =  i;
    numberOfCells=numberOfCells +  1;
    elementTemp =retrievenodetempNEW(sensorElem);
    var t_c = elementTemp+273.15;

    var  a = N_s*n_I*k*t_c/q;
    var  I_L = S_Sref*(I_L_ref+alpha_Isc*(t_c-T_C_ref)); //eq 11
    var E_g_Tc = E_g_tref*(1-0.0003174*(t_c-T_C_ref)); // Duffie & Beckman
    var I_O = I_O_ref*((t_c/T_C_ref)^3)*Math.exp((1/k)*(E_g_tref/T_C_ref-
E_g_Tc/t_c));// Duffie & Beckman


    var I=Imp;
    var v = 0;
    var error = 5;
    while ((Math.abs(error) > 0.01) && (Math.abs(error)<100))
    {
            v=v+0.001;
            error = I_L - I_O*(Math.exp((v+I*R_S)/a)-1)-(v+I*R_S)/R_SH - I; //eq 1
    }
    PendIter=I*v;
    if (Math.abs(error)>100)
    {
            if (error>0){
               System.print("Error too large" + error + " Second   " );
            }
            else{
               PendIter=0;
               System.println("Set power to zero... " + v);
            }
    }
    api.setImposedHeat(sensorElem-1,  -PendIter);
    totalPower = totalPower + PendIter;
    SaveCellPower.push(PendIter);
```

```
                }
    }
    GlobalTotalPower=totalPower;
    GlobalSaveCellPower = SaveCellPower;
}

function printtotalPower()//Prints the power output of the PV-module in the end of each time step
{
    System.println("Total P (T dep): " + GlobalTotalPower);
    System.println("Total P (T ave): " + PaverageTemp);
    System.println("S/Sref:          " + S_Sref);
    System.println("Imp:             " + Imp);
    System.println("-----------------------------------------");
    SummedPdep = SummedPdep + GlobalTotalPower;
    SummedPave = SummedPave + PaverageTemp;
    N_iter = N_iter+1;
    System.println(GlobalSaveCellPower);
}

// If a global variable is not initializes, an error message is printed to the console window.
function initializeSolutionStart()
{
    temp=1;
    irradiation=1;
    averageTemp=1;
    IRRAD=0.0001;
    Imp = 0.0001;
    S_Sref=1;
    GlobalTotalPower = 0.0001;
    PaverageTemp=0.0000000000000001;
    SummedPdep = 0;
    SummedPave=0;
    N_iter=0;
    GlobalSaveCellPower=[];
    elements = [1, 10, 41, 50, 71, 80, 101, 110, 131, 140, 161, 170]; //The elements representing cells
    Pwater = 0;
```

```
//  Constants------
   Gref = 1000; // (W/m2)
   k = 1.381e-23;
   q = 1.60218e-19;
   T_C_ref = 25+273.15;
   N_s = 1;
   E_g_tref = 1.794e-19;//1.12;

   // Single diode parameters
   n_I = 1.2; //1.2 is usual ideality factor Bellia, et al, 2014
   I_L_ref = 9.0507;
   I_O_ref = 1.0888e-8;
   R_S = (0.2553)/60;
   R_SH = (3.3631e3)/60;
   alpha_Isc = 0.0006;



//  Reference values end------
   if
((temp>0)&&(irradiation>0)&&(averageTemp>0)&&(Imp>0)&&(IRRAD>0)&&(Gref>0)&&(S_Sref>0
)&&(GlobalTotalPower>0)&&(PaverageTemp>0));
   else
   {
                System.println( "Error: Failed to initialize ALL global variables." );
                System.println( "  See the documentation for this script" );
   }
}

function CalcAveP()
{
   AveragePdep = SummedPdep/N_iter;
   AveragePave = (SummedPave/N_iter);
   AveragePwater = Pwater/N_iter;
   System.println("########################################");
   System.println("###   Average temp dep P:     " + AveragePdep);
   System.println("###   Average uniform temp P: " + AveragePave);
```

```
    System.println("###   Average thermal P:       " + AveragePwater);
    System.println("########################################");
    System.println("PVTserialDuct_WIND_15.tdf");
}

function getinletoutlettemp()
{
    var sensorElem = 250;
    var outletTemp = retrievenodetempNEW(sensorElem);
    Pwater = Pwater + 1000*(0.5/(60*1000))*4185.5*(outletTemp-10);
    System.println("Thermal Power: " + Pwater);

    }
```